Optics Letters

Nonuniform depolarization properties of typical nanostructures and potential applications

Zhengqiong Dong,[1] Honggang Gu,[2,3] Jinlong Zhu,[2,4] Yating Shi,[2] Lei Nie,[1] Jiaying Lyu,[1] Xiuguo Chen,[2] Hao Jiang,[2] and Shiyuan Liu[2]

[1]Hubei Key Laboratory of Manufacture Quality Engineering, Hubei University of Technology, Wuhan, Hubei 430068, China
[2]State Key Laboratory of Digital Manufacturing Equipment and Technology, Huazhong University of Science and Technology, Wuhan, Hubei 430074, China
[3]e-mail: honggganggu@hust.edu.cn
[4]e-mail: 414180314@qq.com

Received 3 February 2020; accepted 27 February 2020; posted 2 March 2020 (Doc. ID 389732); published 23 March 2020

Nonuniform depolarization properties of SiO_2 thin film, two-dimensional (2D) Si grating, and three-dimensional Si cylinder grating, were systematically investigated by Lu-Chipman decomposition. We find that introducing surface profiles with dimensions comparable to the detecting wavelengths can lead to obvious nonuniform depolarization, and control of the sample azimuth can manipulate the uniformity of the depolarizer components. The results indicate that the 2D nanostructure shows obvious nonuniform depolarization at 0° and 90° azimuths, while almost uniform depolarization at 45° azimuth. These discovered phenomena may give rise to some potential applications, such as the detection of the existence of nanostructures without *a priori* information about the sample, and the design of a uniform or nonuniform depolarizer.

https://doi.org/10.1364/OL.389732

Depolarization, which refers to the coupling of polarized light into unpolarized light [1], is ubiquitous when polarized light passes through an optical medium or system [2–5]. Depolarization is related to the spatial or temporal incoherence of light [6]. Several physical phenomena, including the inhomogeneous distribution in geometric sizes or optical indices of samples [2,3,7], variations in incidence and wavelength induced by the numerical aperture and the finite bandwidth [3,4,8,9], backside reflection from a weak absorption substrate [10], and scattering from inhomogeneous media, such as biological tissues [5,11–14], which account for the optical depolarization, have been reported. Because the above depolarization sources are not negligible in practice, it is necessary to quantitatively characterize the depolarization effect using some mathematic metrics. Under the framework of Stokes-Mueller formalism, several metrics have been proposed to characterize the depolarization effect of an optical system or a medium, typically including the DI [15] (also refers to the degree of polarization [1,16,17] and depolarization purity [6,18,19]), the DP [20], the average degree of polarization [1], the Q metric [21], and the integral and differential DI [22,23]. By these metrics, successful applications including biomedical diagnosis [5,11–13], nanostructure detection [4,9], and optical coherence tomography [16,17,24] were reported recently. Most of the above applications are based on the size of depolarization metrics, but few of them concentrate on the inherent properties of the depolarizer component of an optical system, such as the uniformity or nonuniformity. On the other hand, sub-wavelength nanostructures have been widely applied for integrated optoelectronics devices [25,26], form-birefringence elements [27–29], photonic crystals [30–33], and metasurfaces [34–36], etc. Although these nanostructures can result in optical depolarization to a large extent, the majority of traceable literatures focuses on their diffraction characteristics [26]. In this Letter, we investigate the depolarization properties of typical nanostructures and give a novel insight for potential applications. The depolarization nonuniformity is introduced as a scalar metric to evaluate the intrinsic depolarization properties concealed in the measured Mueller matrices of the nanostructure samples.

To give a clear impression on the uniformity or nonuniformity of the depolarization effect, we take the Mueller matrix of a general depolarizer as an example, which has the following form [20]:

$$\mathbf{M}_\Delta = \begin{bmatrix} 1 & \vec{0}^{\mathrm{T}} \\ \vec{P}_\Delta & \mathbf{m}_\Delta \end{bmatrix}. \tag{1}$$

Here $\vec{P}_\Delta$ is the polarization vector of the depolarizer, and $\mathbf{m}_\Delta$ is a 3×3 symmetric matrix with diagonal elements represented by a, b, and c. For a pure depolarizer, $\vec{P}_\Delta = \vec{0}$ and off-diagonal elements of $\mathbf{m}_\Delta$ are zero [37], leaving only a, b, and c nonzero. The practical Mueller matrix of an optical system, however, is usually far more complex than a pure depolarizer. Some useful Mueller matrix decomposition techniques can be used to extract and analyze the depolarizer features of a practical system. Among these techniques, the Lu-Chipman decomposition [20] is the most widely used one, in which an arbitrary Mueller matrix can be decomposed as

$$\mathbf{M} = \mathbf{M}_\Delta \mathbf{M}_{\mathrm{R}} \mathbf{M}_{\mathrm{D}}. \tag{2}$$

Herein, $\mathbf{M}_D$ is a diattenuator, $\mathbf{M}_R$ is a retarder, and $\mathbf{M}_\Delta$ is the general depolarizer that has the form shown in Eq. (1).

Here the Lu-Chipman decomposition is used to investigate the depolarization properties of typical nanostructures. If the diagonal elements of $\mathbf{m}_\Delta$ satisfy $a = b = c$, we say the general depolarizer is uniform, otherwise nonuniform. We find that the depolarization uniformity varies regularly with the geometrical profiles of the nanostructures. With Lu-Chipman decomposition, we can obtain a general depolarizer without diattenuation or retardance from an arbitrary Mueller matrix. We define quasi-depolarization power (DP) and quasi-depolarization index (DI) for a general polarizer by referencing the actual DP and DI for a pure depolarizer, i.e.,

$$\mathrm{DP} = 1 - \frac{|a+b+c|}{3}, \tag{3a}$$

$$\mathrm{DI} = \sqrt{\frac{a^2+b^2+c^2}{3}}, \tag{3b}$$

where $0 \le \mathrm{DP}, \mathrm{DI} \le 1$. DP and DI can also be utilized to characterize the uniformity of a general depolarizer. This is because Cauchy–Schwartz inequality indicates that

$$\sqrt{\frac{a^2+b^2+c^2}{3}} \ge \frac{|a+b+c|}{3}, \tag{4}$$

where the equality holds only for $a = b = c$. Thus, if $\mathrm{DP} + \mathrm{DI} = 1$ holds, the depolarizer is uniform; otherwise, $\mathrm{DP} + \mathrm{DI} > 1$ indicates that the depolarizer is nonuniform. To characterize the magnitude of the nonuniformity, we set the diagonal elements of $\mathbf{m}_\Delta$ as a depolarization point (a, b, c) in the XYZ Cartesian coordinate system. Note that for a uniform depolarizer, the corresponding coordinate (a, b, c) is on the line $X = Y = Z$, while for a nonuniform depolarizer it deviates from the line $X = Y = Z$. Thus, it is conceivable to take the distance between the point (a, b, c) and line $X = Y = Z$ as the metric to characterize the magnitude of the nonuniformity. We define the nonuniformity metric of the depolarizer as

$$\mathrm{NUM} = \frac{\sqrt{(a-b)^2 + (c-b)^2 + (a-c)^2}}{\sqrt{3}}. \tag{5}$$

The above theory and predefined metrics provide us a novel access to investigating the depolarization nonuniformity in optical systems. In this Letter, we prepared three samples, including a SiO_2 thin film on silicon substrate with a nominal thickness of 100 nm, a two-dimensional (2D) etched silicon trapezoidal grating with its cross-sectional SEM (Nova NanoSEM450, FEI Co.) image and the geometrical description shown in Fig. 1(a), and a three-dimensional (3D) etched silicon cylinder array with the top-down SEM image and geometrical description shown in Fig. 1(b). A commercial Mueller matrix ellipsometer (ME-L ellipsometer, Wuhan Eoptics Technology Co., China) based on the dual-rotating compensator principle [38,39], is utilized to measure the Mueller matrices of the samples. The experiments are carried out over the wavelength range of 300–800 nm with a resolution of 1 nm at the reflective measurement mode with the 65° incidence. In this Letter, the sample azimuth ϕ is defined by the angle between the normal of the incidence plane and the grating lines, as shown in Fig. 1(a). To verify the depolarization

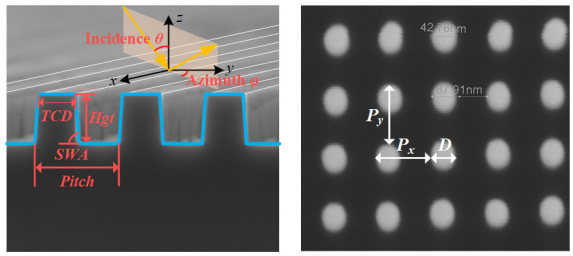

Fig. 1. (a) Cross-sectional SEM image of 2D etched silicon gratings geometrically described by 350 nm TCD, 472 nm Hgt, 86° SWA, and 800 nm Pitch. (b) Top-down SEM image of 3D etched Si cylinder gratings geometrically described by nominal 38 nm diameter D, 90 nm pitch P_x along the X axis, 90 nm pitch P_y along the Y axis, and 420 nm height H.

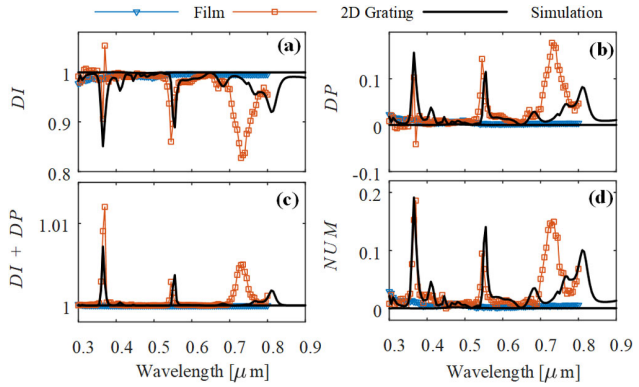

Fig. 2. Depolarization metrics (a) DI, (b) DP, (c) DI + DP, and (d) NUM of depolarizer components for the 2D silicon grating and the 100 nm SiO_2 thin film calculated from measured and simulated Mueller matrices.

phenomena from a point of theory, simulations on the SiO_2 thin film and 2D grating are performed by using the transfer matrix method and the rigorous coupled-wave analysis algorithm, respectively [4]. In simulations, the geometric parameters of the film and grating are set with their nominal values, and the bandwidth and numerical aperture are 1.0 nm and 0.035, respectively, which are calibrated by a standard sample for the ellipsometer. A rectangular function is chosen for calculating the bandwidth and numerical aperture [4].

Figure 2 shows the depolarization metrics DI, DP, DI + DP and NUM for the 2D silicon grating and the SiO_2 thin film calculated from measured and simulated Mueller matrices at 0° azimuth. We find that the 2D grating exhibits obvious depolarization at specific wavelengths, while the thin film shows nearly non-depolarization over the whole wavelength range. Since the experimental conditions, including the bandwidth and the numerical aperture, are the same, the noticeable depolarization should be induced by the 2D grating, which can be regarded as an uneven profile in some sense. The differences between the positions, shapes, and magnitudes of these depolarization peaks in the experimental spectra and those in the simulated ones mainly come from the differences in the geometric parameters and conditions in the simulations compared to their practical values in the experiments.

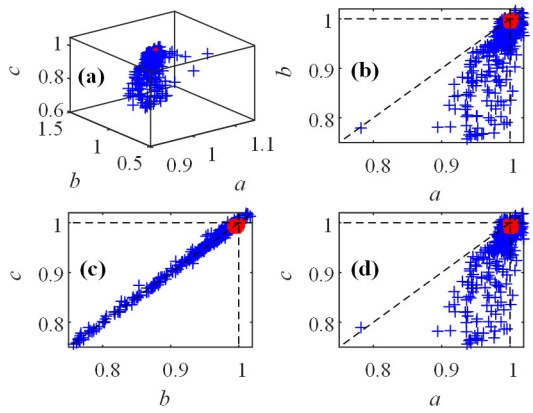

Fig. 3. Depolarization points in (a) Cartesian coordinate system and projections on planes of (b) ab, (c) bc, and (d) ac. The red squares and blue crosses are for data of the SiO_2 film and the 2D Si grating, respectively.

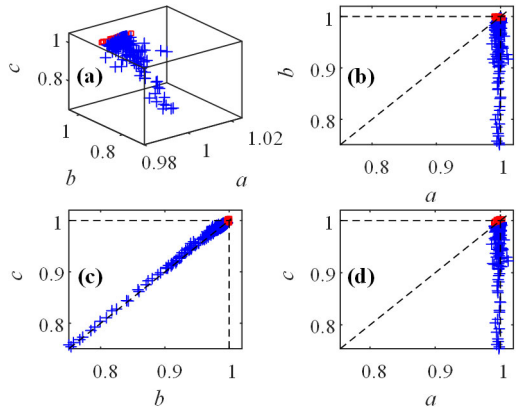

Fig. 4. Depolarization points in (a) a Cartesian coordinate system and projections on planes of (b) ab, (c) bc, and (d) ac. The red squares and blue crosses are for data of the SiO_2 film and the 3D Si cylinder, respectively.

From Figs. 2(c) and 2(d), we can observe that the 2D Si grating introduces obvious nonuniform depolarization mainly around 380, 550, and 750 nm. To further reveal the nonuniform depolarization, we depict the depolarization points (a, b, c) and their projections at each wavelength in the Cartesian coordinate system, as shown in Fig. 3. It can be seen from Fig. 3(a) that the depolarization points of the thin film are nearly all concentrated on the point (1, 1, 1), while those of the 2D grating distribute over a larger vicinity around the point (1, 1, 1), indicating that the thin film only causes very weak and uniform depolarization. Despite those physically unrealizable points (whose elements are larger than 1) caused by experimental errors and noises, the projections of depolarization points of the 2D grating on a bc plane nearly all lie on the line $b = c$. While on ab and ac planes, the projections are nearly all around $a = 1$. This implies that for the 2D grating we have $a > b = c$. To further illustrate this conclusion, we also consider the case of the 3D Si cylinder array. The same situations can be found in Fig. 4, i.e., the 3D cylinder grating also satisfies $a > b = c$. Different from the 2D grating, for the 3D cylinder array, the projections on ab and ac planes are nearly strictly lying on the vertical line $a = 1$.

The above experiments demonstrate that nanostructures, such as 2D and 3D gratings, induce strong nonuniform depolarization that is different from the thin film. One question is, "does the relation $a > b = c$ always hold for these 2D or 3D nanostructures?" To give an answer, we measured the Mueller matrices of the 2D grating at different azimuths, as it is more sensitive to the azimuth than the other two samples.

As shown in Fig. 5, the azimuth has significant effects on the depolarization properties of the 2D Si gratings, including positions, shapes, and magnitudes of depolarization peaks. With the azimuth increasing, the DI exhibits an obvious increase, while the NUM presents a non-monotonous change, which has a trend $90° > 0° > 45°$ in the concerned wavelength range. In addition, the NUM peaks at 45° azimuth seem more concentrated and sharper than those at 0° and 90° azimuths.

To more clearly demonstrate the effect of the azimuth on the NUM, we plotted the projections of the depolarization points obtained at 0°, 45°, and 90° azimuths on the plane of ab, bc, and ac, respectively, from a statistical perspective, as shown in

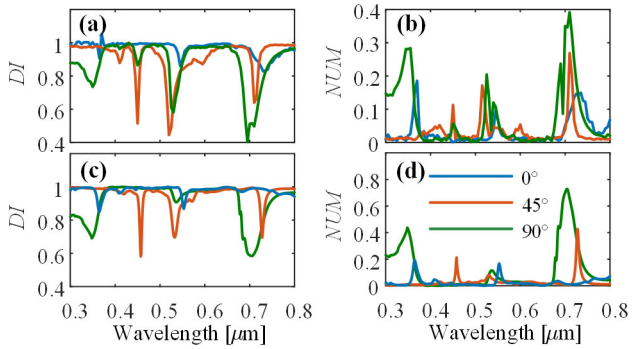

Fig. 5. DI and NUM of the depolarization components of the 2D grating at 0°, 45°, and 90° azimuths: (a) (b) experiments; (c), (d) simulations.

Fig. 6. It can be seen that the relation $b = c$ is always fulfilled for all the azimuths. For 45° azimuth, we can obviously find that most projections of the depolarization points lie on the lines $a = b$ and $a = c$, as shown in Figs. 6(d) and 6(f). This indicates that the 2D grating presents uniform depolarization over most wavelengths at 45° azimuth. While for 0° and 90° azimuths, it presents nonuniform depolarization, and the relation $a > b = c$ is fulfilled, since the projection points in Figs. 6(a), 6(c), 6(g), and 6(i) are nearly below the angular bisectors, while those in Figs. 6(b) and 6(h) nearly all locate on the angular bisector.

Inspired by the above results and discussion, we can expect some potential applications with the nonuniform depolarization properties of nanostructures. For example, by detecting the NUM peaks, one can judge the existence and types of nanostructures without any *a priori* information, and evaluate the dimensions and orientations of nanostructures roughly. The relations between the depolarization properties and the dimensions and orientations of nanostructures revealed by us can help to design different uniform or nonuniform depolarizers based on nanostructures, such as the multi-band depolarizer.

In this Letter, we systematically investigate the nonuniform depolarization properties of the SiO_2 thin film, 2D etched Si grating, and 3D etched Si cylinder grating. We find that the

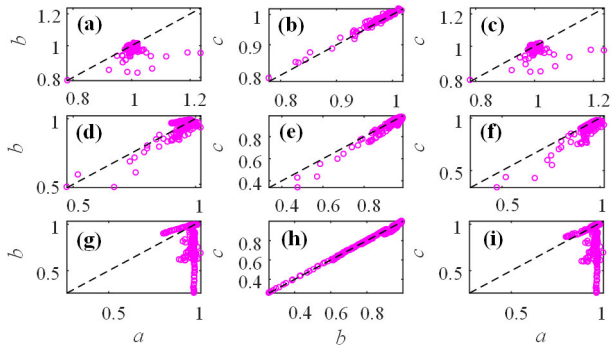

Fig. 6. Projections of the depolarization points of the 2D etched Si grating on the three coordinate planes ab, bc, and ac. Subfigures (a)–(c), (d)–(f), and (g)–(i) correspond to the results obtained at 0°, 45°, and 90° azimuthal angles, respectively.

introduction of surface profiles with dimensions comparable to the detecting wavelength can lead to nonuniform depolarization. Moreover, by changing the azimuths of the nanostructures, we can manipulate the uniformity of the depolarization, and the approximately uniform depolarization property can be obtained at 45° azimuth. These phenomena may give rise to some potential applications, such as the detection and classification of nanostructures without any *a priori* information, and the control and design of a uniform or nonuniform depolarizer with nanostructures.

Funding. National Natural Science Foundation of China (51525502, 51727809, 51805193, 51975191); Natural Science Foundation of Hubei Province (2018CFB290, 2018CFB559); China Postdoctoral Science Foundation (2016M602269, 2016M602288, 2017T100546, 2019M652633); National Major Science and Technology Projects of China (2017ZX02101006-004).

Disclosures. The authors declare no conflicts of interest.

REFERENCES

1. R. A. Chipman, Appl. Opt. **44**, 2490 (2005).
2. J. Lee, P. I. Rovira, I. An, and R. W. Collins, Rev. Sci. Instrum. **69**, 1800 (1998).
3. S. Zollner, T.-C. Lee, K. Noehring, A. Konkar, N. D. Theodore, W. M. Huang, D. Monk, T. Wetteroth, S. R. Wilson, and J. N. Hilfiker, Appl. Phys. Lett. **76**, 46 (2000).
4. X. Chen, C. Zhang, and S. Liu, Appl. Phys. Lett. **103**, 151605 (2013).
5. W. Sheng, W. Li, J. Qi, T. Liu, H. He, Y. Dong, S. Liu, J. Wu, D. S. Elson, and H. Ma, Photonics **6**, 34 (2019).
6. A. V. Eeckhout, A. Lizana, E. Garcia-Caurel, J. J. Gil, R. Ossikovski, and J. Campos, Opt. Lett. **42**, 4155 (2017).
7. U. Richter, Thin Solid Films **313**, 102 (1998).
8. S. F. Nee, J. Opt. Soc. Am. A **17**, 2067 (2000).
9. L. H. Herman, C. J. Kim, Z. Wang, M. H. Jo, and J. Park, Appl. Phys. Lett. **101**, 123102 (2012).
10. R. Joerger, K. Forcht, A. Gombert, M. Kohl, and W. Graf, Appl. Opt. **36**, 319 (1997).
11. W. Groner, J. W. Winkelman, A. G. Harris, C. Ince, G. J. Bouma, K. Messmer, and R. G. Nadeau, Nat. Med. **5**, 1209 (1999).
12. N. Ortega-Quijano, F. Fanjul-Velez, J. D. Cos-Perez, and J. L. Arce-Diego, Opt. Commun. **284**, 4852 (2011).
13. J. Golde, F. Tetschke, J. Walther, T. Rosenauer, F. Hempel, C. Hannig, E. Koch, and L. Kirsen, J. Biomed. Opt. **23**, 071203 (2018).
14. A. V. Eeckhout, E. Garcia-Caurel, T. Garnatje, M. Durfort, J. C. Escalera, J. Vidal, J. J. Gil, J. Campos, and A. Lizana, PLoS ONE **14**, e0213909 (2019).
15. J. J. Gil and E. Bernabeu, Opt. Acta **33**, 185 (1986).
16. S. Makita, Y. J. Hong, M. Miura, and Y. Yasuno, Opt. Lett. **39**, 6783 (2014).
17. N. Lippok, M. Villiger, and B. E. Bouma, Opt. Lett. **40**, 3954 (2015).
18. A. Tariq, P. Li, D. Chen, D. Lv, and H. Ma, Phys. Rev. Lett. **119**, 033202 (2017).
19. A. Tariq, H. He, P. Li, and H. Ma, Opt. Express **27**, 22645 (2019).
20. S. Y. Lu and R. A. Chipman, J. Opt. Soc. Am. A **13**, 1106 (1996).
21. R. Espinosa-Luna, E. Bernabeu, and G. Atondo-Rubio, Appl. Opt. **47**, 1575 (2008).
22. R. Ossikovski and O. Arteaga, Opt. Lett. **40**, 954 (2015).
23. N. Ortega-Quijano, F. Fanjul-Velez, and J. L. Arce-Diego, Opt. Lett. **40**, 3280 (2015).
24. N. Ortega-Quijano, T. Marvdashti, and A. K. E. Bowden, Opt. Lett. **41**, 2350 (2016).
25. C. J. Chang-Hasnain and W. Yang, Adv. Opt. Photonics **4**, 379 (2012).
26. N. G. Orji, M. Badaroglu, B. M. Barnes, C. Beitia, B. D. Bunday, U. Celano, R. J. Kline, M. Neisser, Y. Obeng, and A. E. Vladar, Nat. Electron. **1**, 532 (2018).
27. F. Xu, R. C. Tyan, P. C. Sun, Y. Fainman, C. C. Cheng, and A. Scherer, Opt. Lett. **20**, 2457 (1995).
28. D. Yi, Y. Yan, H. Liu, S. Lu, and G. Jin, Opt. Lett. **29**, 754 (2004).
29. M. T. Posner, N. Podoliak, D. H. Smith, P. L. Mennea, P. Horak, C. B. E. Gawith, P. G. R. Smith, and J. C. Gates, Opt. Express **27**, 11174 (2019).
30. K. Busch, G. V. Freymann, S. Linden, S. F. Mingaleev, L. Tkeshelashvili, and M. Wegener, Phys. Rep. **444**, 101 (2007).
31. G. V. Freymann, A. Ledermann, M. Thiel, I. Staude, S. Essig, K. Busch, and M. Wegener, Adv. Funct. Mater. **20**, 1038 (2010).
32. F. Priolo, T. Gregorkiewicz, M. Galli, and T. F. Krauss, Nat. Nanotechnol. **9**, 19 (2014).
33. P. Qiao, W. Yang, and C. J. Chang-Hasnain, Adv. Opt. Photonics **10**, 180 (2018).
34. B. Lukyanchuk, N. I. Zheludev, S. A. Maier, N. J. Halas, P. Nordlander, H. Giessen, and C. T. Chong, Nat. Mater. **9**, 707 (2010).
35. A. I. Kuznetsov, A. E. Miroshnichenko, M. L. Brongersma, Y. S. Kivshar, and B. Luk'yanchuk, Science **354**, aag2472 (2016).
36. J. M. Luque-Gonzalez, A. Herrero-Bermello, A. Ortega-Monux, I. Molina-Fernandez, A. V. Velasco, P. Cheben, J. H. Schmid, S. Wang, and R. Halir, Opt. Lett. **43**, 4691 (2018).
37. C. Fallet, A. Pierangelo, R. Ossikovski, and A. D. Martino, Opt. Express **18**, 831 (2010).
38. H. Gu, X. Chen, H. Jiang, C. Zhang, and S. Liu, J. Opt. **18**, 025702 (2016).
39. S. Liu, X. Chen, and C. Zhang, Thin Solid Films **584**, 176 (2015).